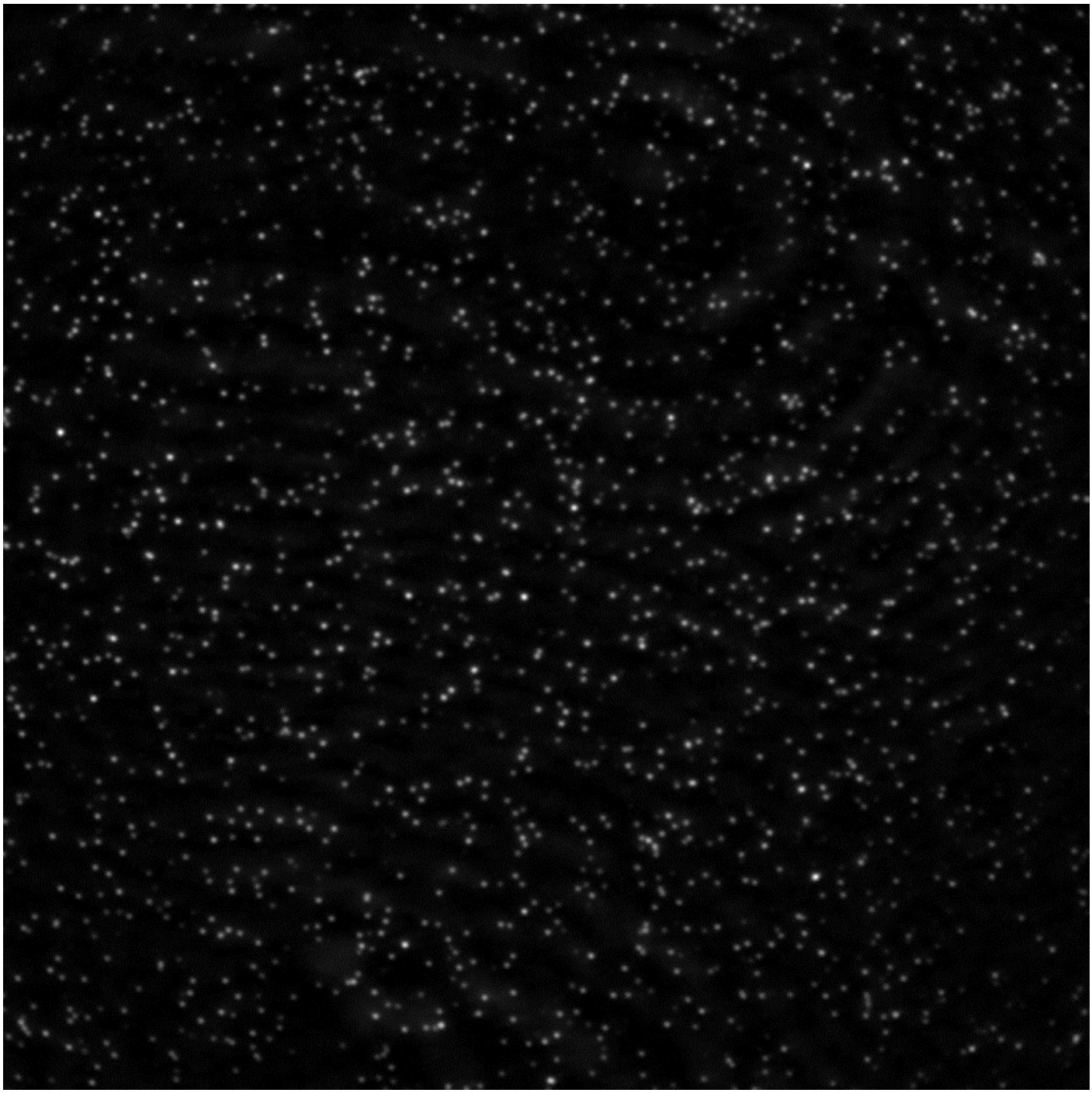

Supplementary Figure 1

Time-averaged fluorescence image showing signal from both specific and nonspecific binding of the fluorescent probe for miR-141.

Individual fluorescent puncta are analyzed for kinetics of probe binding to distinguish between signal from genuine targets and background binding (Fig. 1a-d).

Nature Biotechnology: doi:10.1038/nbt.3246

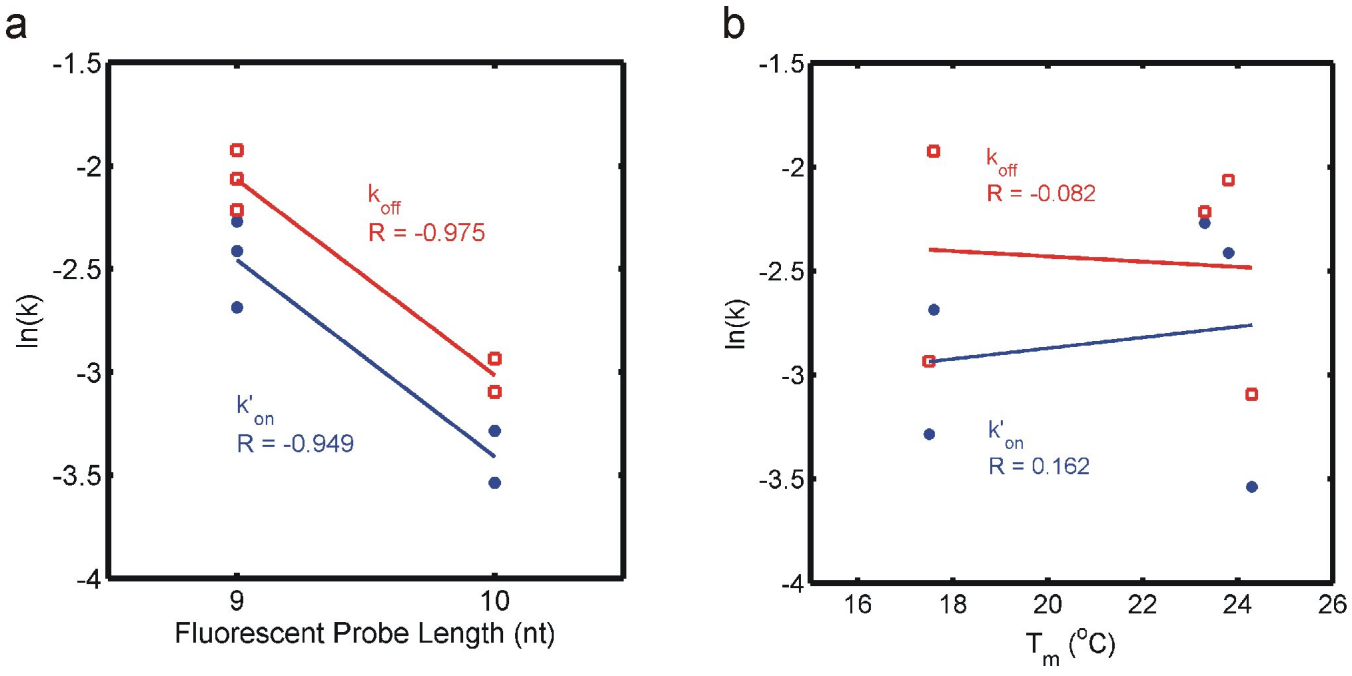

Supplementary Figure 2

Impact of probe length and T_m on kinetics.

a, There is strong negative correlation between the length of the fluorescent probe and the measured dissociation rate constant (k_{off}) as well as the pseudo-first-order association rate constant (k'_{on}). While an increase in k_{on} for shorter probes is perhaps intuitively surprising, similar trends have been reported in single-molecule studies by other labs within this range of duplex lengths[22,23]. **b,** In contrast, no significant correlation is evident between the theoretically predicted T_m of the probe-target duplexes and the rate constants of binding or dissociation. T_m values were predicted using the OligoAnalyzer application from Integrated DNA Technologies using the following parameters: target type = RNA, oligonucleotide concentration = 25 nM, Na+ concentration = 600 mM, Mg++ concentration = 0. ˚

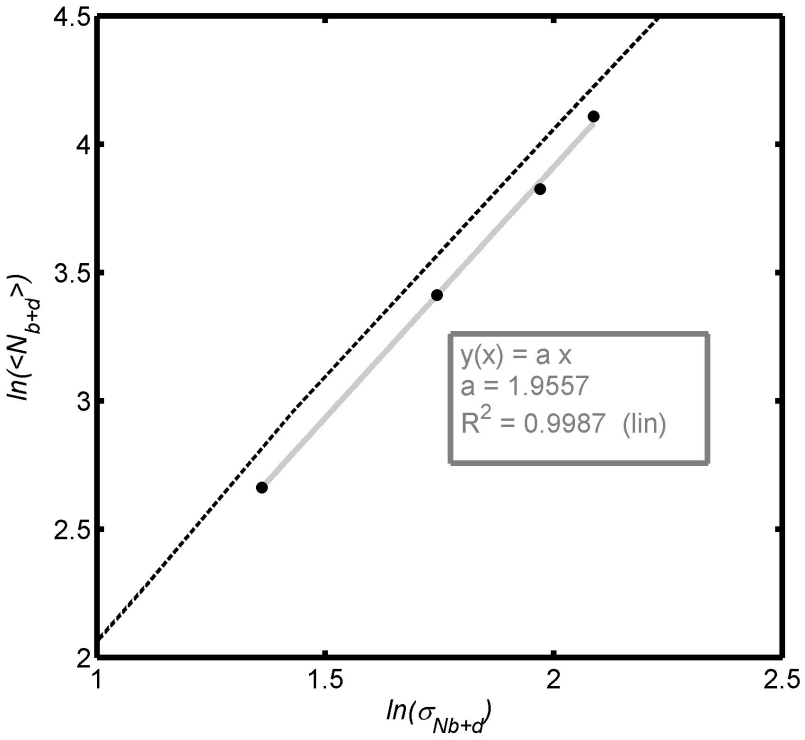

Supplementary Figure 3

$\sigma_{N_{b+d}}$ increases as $\sqrt{N_{b+d}}$

The standard deviation in the number of binding/dissociation transitions per molecule, $\sigma_{N_{b+d}}$, is plotted against the mean number of transitions per molecule, $<N_{b+d}>$, on a log-log scale. Both experimental data for *hsa-miR-141* (black circles) and simulations with $k'_{on} = k_{off} = 6$ min^{-1} (dashed line) are shown for comparison. A linear regression fit to the experimental data yields a slope of ~2, showing that $\sigma_{N_{b+d}}$ increases as $\sqrt{N_{b+d}}$, as expected for a Poisson process.

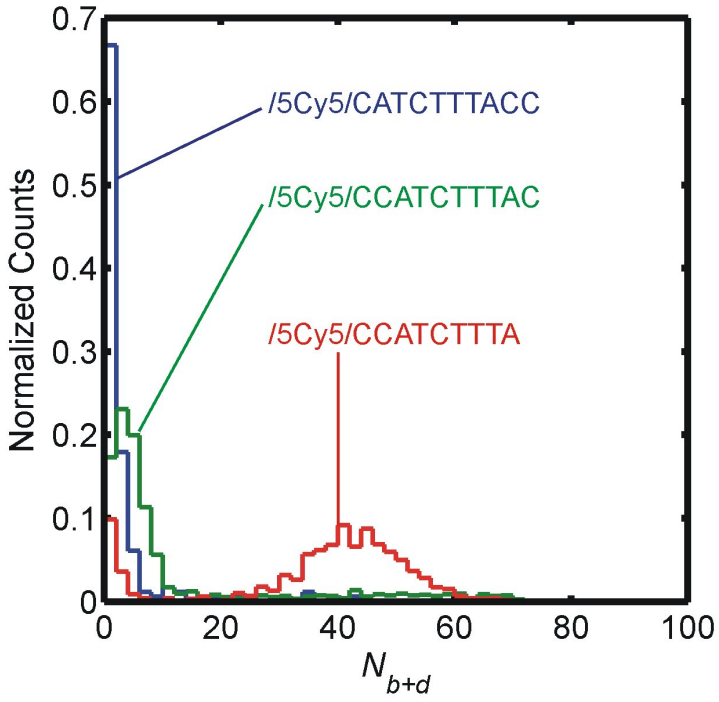

Supplementary Figure 4

Optimization of the fluorescent probe for miR-141

While both 10-nucleotide probes yielded poor separation between signal and background, reducing the length of the probe to 9 nt yielded a distinct signal peak.

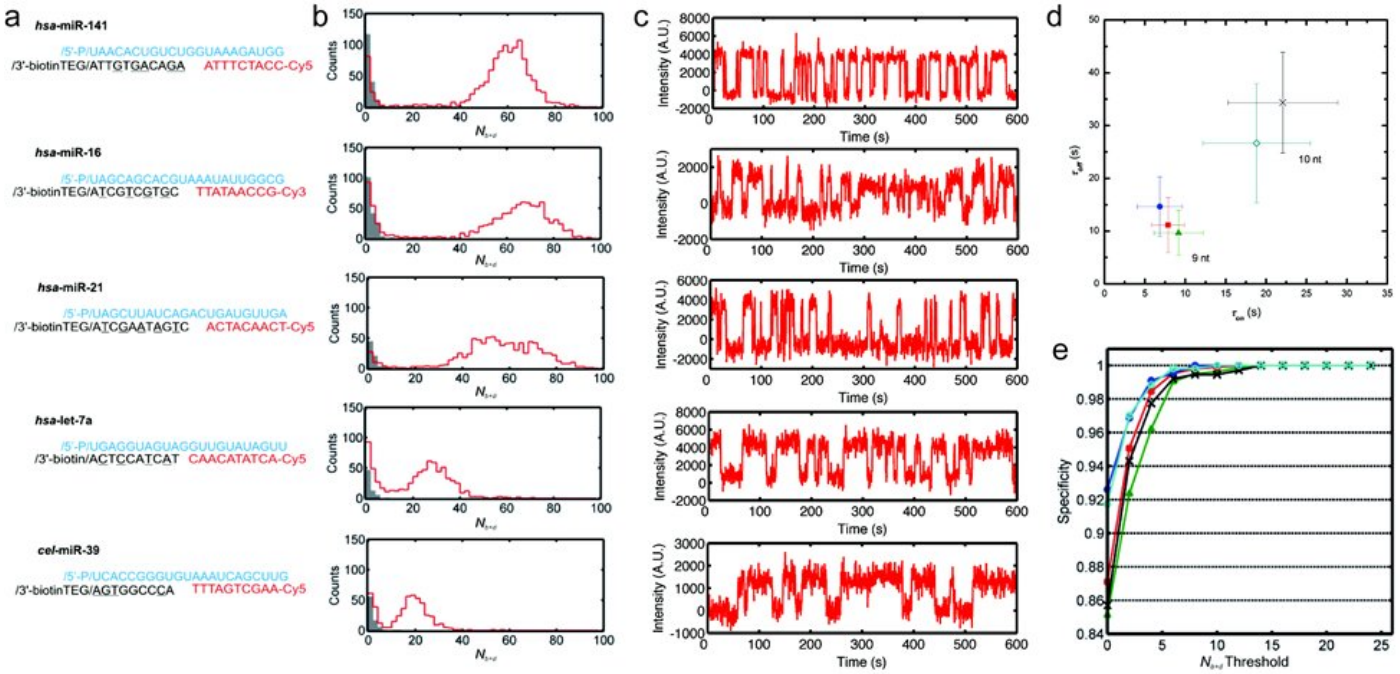

Supplementary Figure 5

Zero-background detection of diverse miRNAs by SiMREPS

a, Probe and target sequences for the detection of four miRNA targets from *H. sapiens* and one from *C. elegans*. The blue sequences represent the miRNA targets, the black sequences represent the locked nucleic acid capture probes, and the red sequences represent the transiently binding fluorescent DNA probes. The underlined letters in the capture probe sequences signify LNA rather than DNA nucleotides. **b**, Histograms of N_{b+d} in the absence (black) or presence (red) of miRNA targets. All targets were present at 1 pM except for *miR-16*, which was present at 500 fM. **c**, Representative fluorescence-*versus*-time trajectories for single immobilized miRNAs using the probes shown in (**a**). **d,** Mean bound (τ_{on}) and unbound (τ_{off}) state lifetimes for the five probe-target pairs shown in (**a**). The symbols correspond to *hsa-miR-141* (red squares), *hsa-let-7a* (cyan diamonds), *hsa-miR-16* (green triangles), *hsa-miR-21* (blue circles), and *cel-miR-39* (black crosses). Error bars represent one standard deviation; it is noted that the lifetimes of the 9- and 10-nucleotide probes cluster in distinct regions of the plot. **e**, Specificity of detection of the five miRNA targets as a function of N_{b+d} threshold. The symbols are the same as in (**d**).

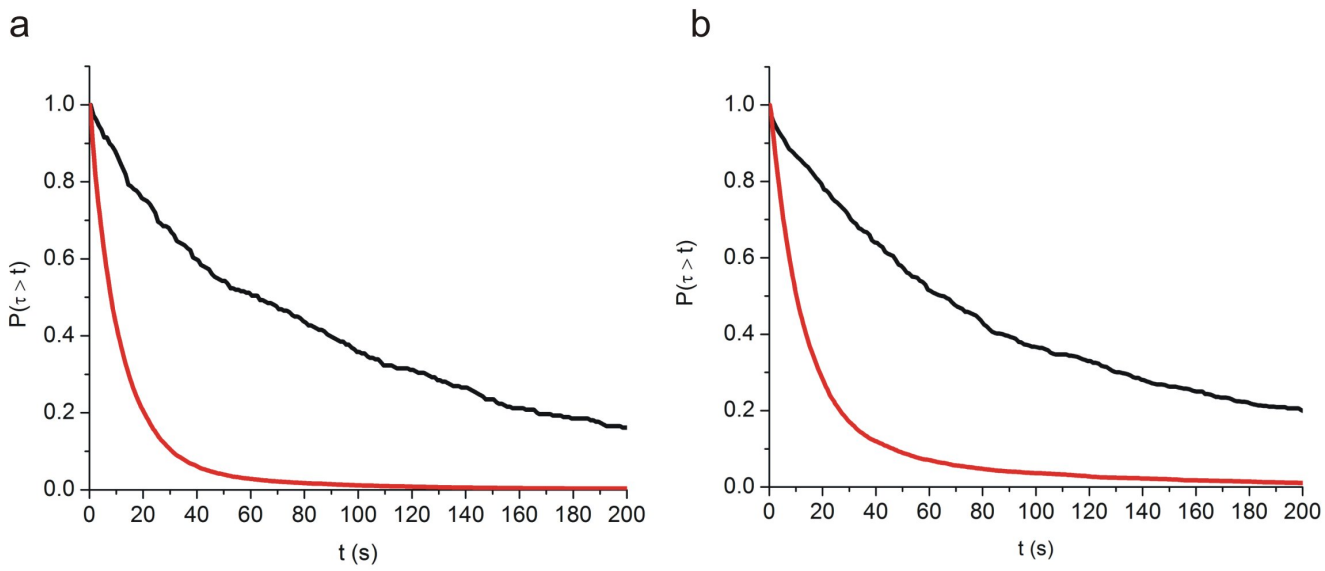

Supplementary Figure 6

On-state dwell time distributions of Cy5 and Cy3 fluorescent probes in presence and absence of target miRNA

a,b On-state dwell time distributions of fluorescent probes for miR-141 (**a**, Cy5-labeled probe) and miR-16 (**b**, Cy3-labeled probe) in the presence (red) and absence (black) of the target miRNA. The dwell time distributions in absence of target (black) likely reflect both photobleaching and dissociation of nonspecifically surface-bound probes, and thus provide lower-bound estimates of the photobleaching time constant for each fluorophore.

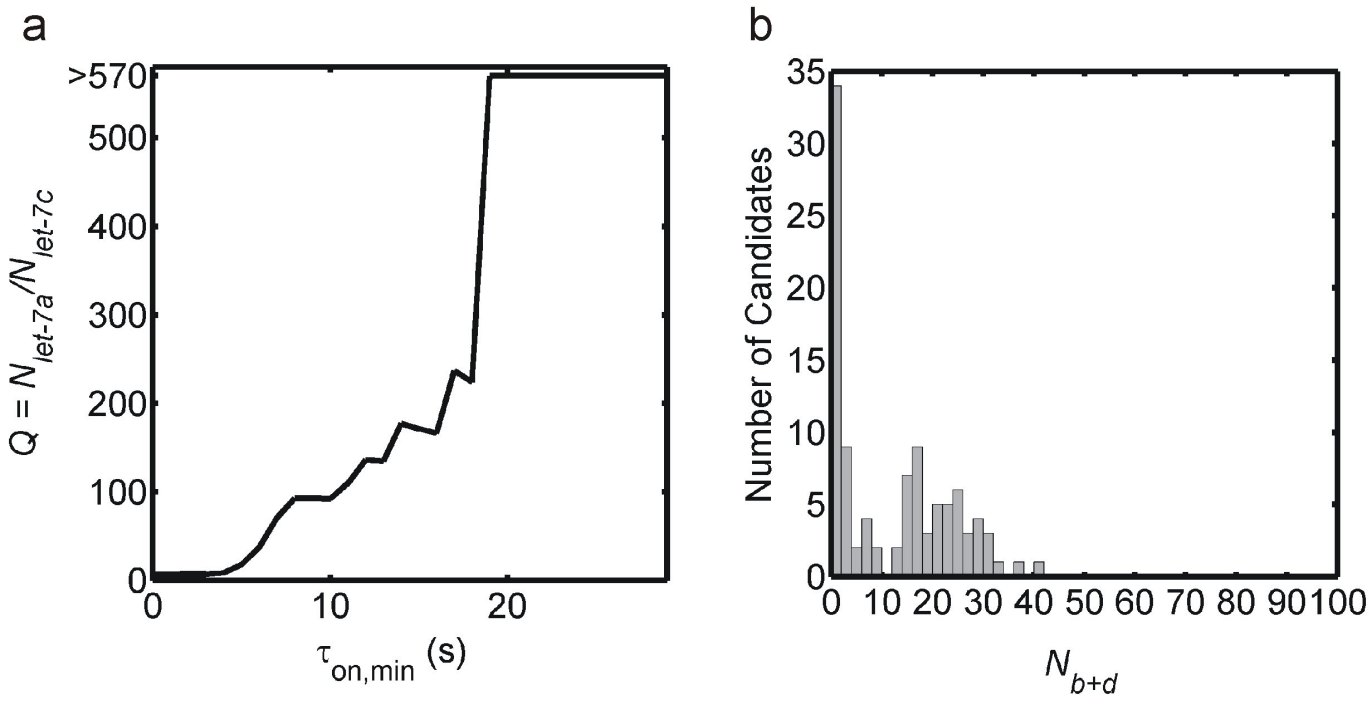

Supplementary Figure 7

let-7a/c discrimination and N_{b+d} histogram of *let-7c*

a, Discrimination factor *Q* describing the specificity of *let-7a* detection over *let-7c* at varying values of the bound-state lifetime threshold, $\tau_{on,min}$. **b,** N_{b+d} histogram for *let-7c* detected using the fluorescent probe for *let-7a*. While the shape of the histogram is similar to that for *let-7a* (Supplementary Fig. 5b), the sensitivity is much lower due to the short binding events, and the two targets can be more completely resolved using their disparate τ_{on} values (panel **a** and Fig. 2).

Nature Biotechnology: doi:10.1038/nbt.3246

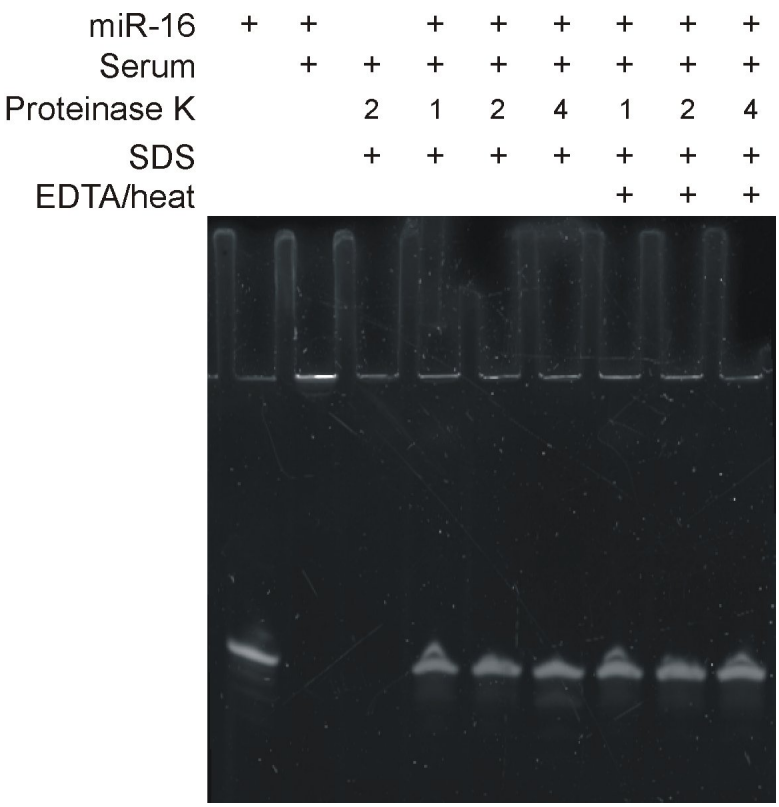

Supplementary Figure 8

Protection of miRNA from degradation in serum using proteinase K and SDS

Synthetic miR-16 is completely degraded by the addition of untreated human serum, but is protected by the simultaneous addition of proteinase K (1, 2, 4 correspond to 0.08, 0.16, or 0.32 units/μL) and SDS. Subsequent heating to 90 °C for 2 min in the presence of 20 mM EDTA does not result in significant degradation.

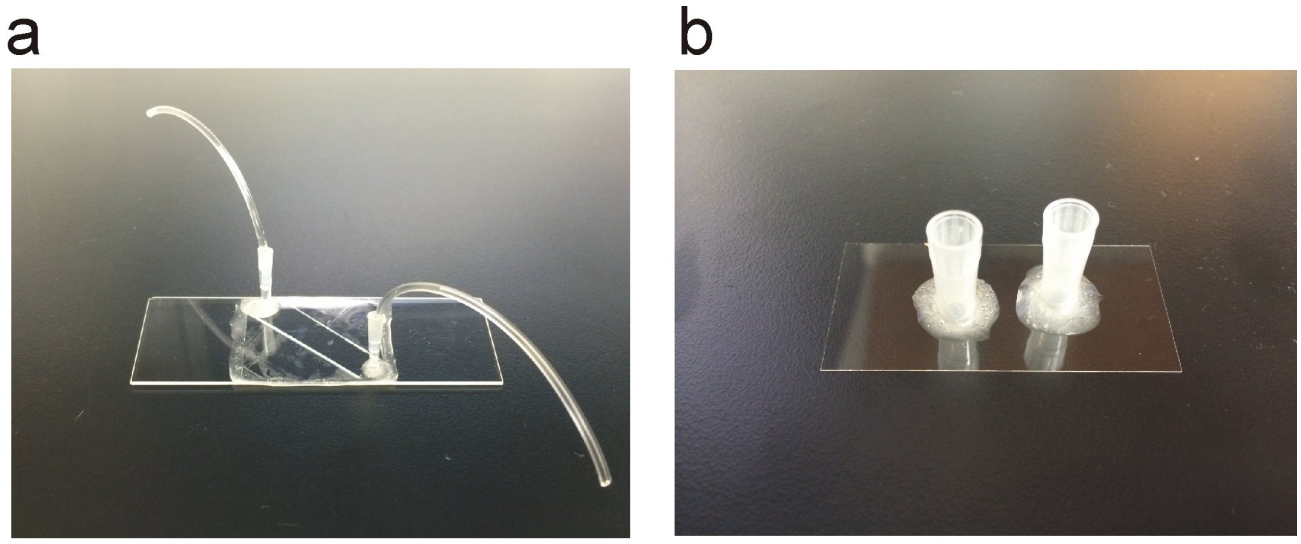

Supplementary Figure 9

Current sample cell designs for SiMREPS using prism-TIRF and objective-TIRF microscopy

a, Closed flow cell constructed for prism-TIRF using double-sided tape sandwiched between a coverslip and a fused silica slide bearing two ~1-mm holes and Tygon tubing for buffer exchange[24]. **b**, Taller objective-TIRF sample cell constructed by fastening a cut pipet tip to a coverslip. This sample cell permits a taller column of fluid (~1 cm), resulting in greater sensitivity than with the prism-TIRF flow cell[11].

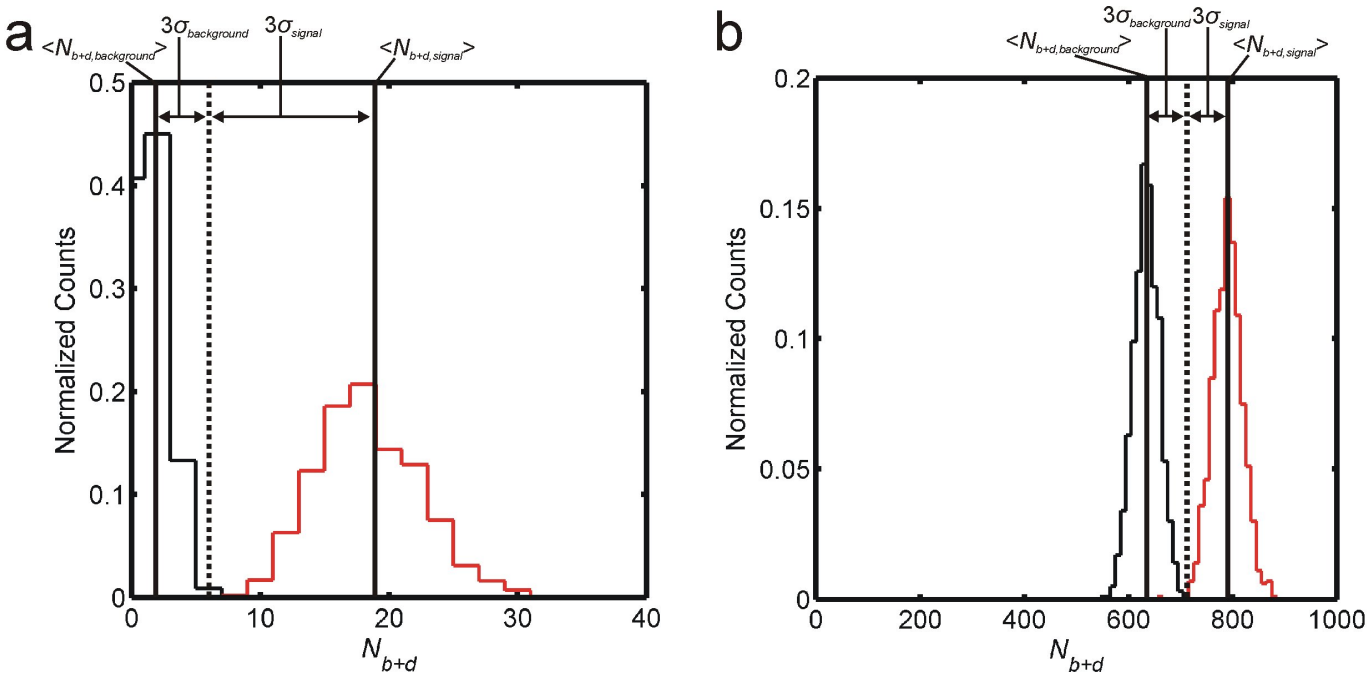

Supplementary Figure 10

Simulated N_{b+d} histograms from kinetic Monte Carlo simulations of SiMREPS probing

a, Signal (red) and background (black) distributions of N_{b+d} from simulations in which $k_{on+off,signal}$ = 5 min^{-1}, $k_{on+off,background}$ = 0.5 min^{-1}, and the simulation time is 3.9 min. **b,** N_{b+d} distributions from simulations in which $k_{on+off,signal}$ = 5 min^{-1}, $k_{on+off,background}$ = 4 min^{-1}, and the simulation time is 161.5 min. In all cases, histograms were constructed from 1,000 individual simulated trajectories.

Nature Biotechnology: doi:10.1038/nbt.3246

Supplementary Note 1: Supporting Discussion

Stable, diagnostically useful miRNAs have recently been detected in several body fluids, including blood[1], saliva, urine, and sputum[2]. However, reproducible extraction and quantification of circulating miRNAs has proven challenging, presumably due to their typically low abundance and frequent association with lipids and proteins[3]. Moreover, standard assays based on amplification by polymerase chain reaction (PCR), while highly sensitive, require time-consuming extraction and amplification steps. While next-generation sequencing approaches provide a powerful high-throughput route to the profiling of RNA transcripts, many of these techniques also suffer from problems such as uneven amplification[4] and inefficient detection of rare species of interest in absence of sufficient sequencing depth,[5] as well as generally high error rates, particularly in the case of single-molecule sequencing[6]. Poor agreement with expression level data using other techniques such as microarrays has also been reported[7]. Barcoding approaches such as molecular indexing[8] improve the accuracy of absolute RNA counting, but are otherwise subject to many of the same problems as other next-generation sequencing techniques. An amplification-free approach to the sensitive and highly specific detection and quantification of miRNAs in minimally treated native biofluids and tissue samples would allow more rapid quantification of these biomarkers, potentially enabling routine point-of-care diagnosis.

Amplification-free detection of short nucleic acid targets typically utilizes thermodynamic discrimination by a nucleic acid probe that hybridizes to a complementary sequence within the target[9–14]. While quite robust and avoiding time-consuming enzymatic amplification, these methods face two main difficulties. First, in absence of amplification, high-sensitivity detection generally requires single-molecule measurements that are frequently hampered by background signal representing a substantial fraction of the positive signal – *i.e.*, incomplete discrimination above background[15,16]. While it is common to subtract such background signal using a blank measurement, this approach is only feasible if the background signal is extremely reproducible and robust to changes in the sample matrix. Second, essentially all existing methods rely on thermodynamic discrimination, which places fundamental limits on the specificity of detection – *i.e.*, incomplete discrimination against spurious targets[14]. Such limits become particularly important in the face of heterogeneous samples containing varying ratios of functionally significant isoforms of a target, such as miRNAs bearing single-nucleotide variations that alter their gene-silencing properties[17]. While amplification-free approaches to RNA quantification using single-molecule sequencing have been reported[18,19], these require RNA isolation and enzymatic steps, and are limited by the high raw error rates that currently characterize single-molecule sequencing.[6,18]

The use of transiently binding probes in SiMREPS bypasses the fundamental limits of discrimination imposed by thermodynamic differences in the context of other amplification-free analytical approaches. As long as there is a slight difference in the kinetics of probe binding or dissociation between a genuine and a spurious target, repeated sampling is theoretically able to resolve them (see Supplementary Note 2 and Supplementary Fig. 9). The SiMREPS technique allows not only the zero-background detection of single RNA molecules, but also the reliable discrimination of single-base mutants, opening up possibilities for the rapid and reliable detection of even scarce single-nucleotide polymorphisms in complex biological specimens. The capacity

to identify and count individual target molecules with high confidence sets SiMREPS apart from other single-molecule kinetic approaches to quantification, which pool kinetic information from an ensemble of surface-bound targets[15], limiting their capacity to distinguish closely related targets in a complex mixture.

Of importance for potential applications in clinical diagnostics, we have demonstrated that SiMREPS can detect spiked-in and endogenous miRNA targets in crude biological specimens following only minimal treatment with SDS and/or proteinase K. In addition to retarding or preventing degradation of the target analytes, these additives may serve to liberate the miRNAs from the protein and lipid complexes with which they are natively associated. Thus, we bypass the more lengthy steps of RNA isolation, reverse transcription, and amplification that are typically required for PCR-based assays of miRNAs, including those involving next-generation sequencing. The rate-limiting step for SiMREPS is presently the passive mass transport of dilute analytes to the surface for capture, which takes ~1 h in our typical flow cell geometry, but can in principle be accelerated by incorporating active mechanical, electrophoretic, or magnetic manipulation. While data analysis is currently only semi-automated, it requires only seconds of computing time and could be fully automated to further streamline the assay pipeline. One current barrier to widespread adoption of SiMREPS may be the price tag of a commercial TIRF microscope, but this is likely reduced with simplified and specialized instrumentation.

While we have restricted our analysis to individual targets in a given specimen, SiMREPS can in principle accommodate various approaches to multiplexing. In addition to the option of utilizing spectrally distinct fluorescent probes to monitor a few targets simultaneously ($\leq$ 4 on most TIRF microscopes), an arbitrary degree of serial multiplexing could be possible by sequential exchange of the transiently binding probes[20]. Still more efficient schemes could be envisioned that exploit spatial segregation of capture strands in printed microarrays, perhaps in conjunction with zero-mode waveguides[21] to suppress background fluorescence from the multiple probes that must be present in the same imaging chamber.

Supplementary Note 2: Theoretical considerations of kinetic discrimination

For two-state binding with fixed rate constants of fluorescent probe (FP) binding ($k_{on}' = k_{on}[FP]$) and dissociation (k_{off}), the expected number of transitions between the bound and unbound state per unit time is:

$$k_{on+off} = k'_{on}\frac{k_{off}}{k'_{on}+k_{off}} + k_{off}\frac{k'_{on}}{k'_{on}+k_{off}}$$

$$= 2\frac{k'_{on}k_{off}}{k'_{on}+k_{off}} \quad (1)$$

where the factors $\frac{k_{off}}{k'_{on}+k_{off}}$ and $\frac{k'_{on}}{k'_{on}+k_{off}}$ represent the fraction of time a molecule spends in the probe-free and probe-bound states, respectively. The expected number of binding and dissociation events observed in a given time window is thus:

$$\langle N_{b+d}\rangle = k_{on+off}t = 2t\frac{k'_{on}k_{off}}{k'_{on}+k_{off}} \quad (2)$$

Therefore, $\langle N_{b+d}\rangle_{background}$ will be a constant fraction f of $\langle N_{b+d}\rangle_{signal}$, where $0 < f < 1$. If we wish to extend the observation window such that $\langle N_{b+d}\rangle$ for signal and background are separated by a given multiple of standard deviations, *e.g.* $3\sigma_{background} + 3\sigma_{signal}$, a minimum acquisition time is necessary. This is given by the inequality:

$$\langle N_{b+d}\rangle_{signal} - \langle N_{b+d}\rangle_{background} \geq 3\sigma_{background} + 3\sigma_{signal} = 3\sqrt{\langle N_{b+d}\rangle_{background}} + 3\sqrt{\langle N_{b+d}\rangle_{signal}} \quad (3)$$

where $\sigma = \sqrt{\langle N_{b+d}\rangle}$. After substituting $f\langle N_{b+d}\rangle_{signal}$ for $\langle N_{b+d}\rangle_{background}$, this inequality can be rearranged to:

$$\langle N_{b+d}\rangle_{signal} \geq 9\frac{(1+\sqrt{f})^2}{(1-f)^2} \quad (4)$$

$$k_{on+off}t \geq 9\frac{(1+\sqrt{f})^2}{(1-f)^2} \quad (5)$$

$$t \geq 9\frac{1}{k_{on+off}}\frac{(1+\sqrt{f})^2}{(1-f)^2} \quad (6)$$

As a concrete example, if $k_{b+d,signal}$ = 5 min^{-1} and $k_{b+d,background}$ = 0.5 min^{-1} (similar to the values we measure for the *miR-141* fluorescent probe in our experiments), the minimum observation time to separate the two measurements is ~3.85 min, which compares favorably with the peak separation shown in Fig. 1d. However, as long as k_{b+d} is not identical for signal and background, it is theoretically possible to achieve arbitrary discrimination with increased acquisition time. For instance, if $k_{b+d,signal}$ = 5 min^{-1} and $k_{b+d,background}$ = 4 min^{-1}, the distributions are predicted to be separate (by a distance of $3\sigma_{background} + 3\sigma_{signal}$) after 161.5 min of observation. Both of the above situations are illustrated using simulated N_{b+d} histograms in Supplementary Figure 9. Also, as we have shown with let-7a/c, it may be possible to resolve two targets based on distinct bound state lifetimes (Fig. 2a-c) even if their N_{b+d} distributions are similar.

Supporting References

1. Mitchell, P. S. *et al.* Circulating microRNAs as stable blood-based markers for cancer detection. *PNAS* **105,** 10513–10518 (2008).
2. Iorio, M. V. & Croce, C. M. MicroRNA dysregulation in cancer: diagnostics, monitoring and therapeutics. A comprehensive review. *EMBO Molecular Medicine* **4,** 143–159 (2012).
3. Schwarzenbach, H., Hoon, D. S. B. & Pantel, K. Cell-free nucleic acids as biomarkers in cancer patients. *Nat Rev Cancer* **11,** 426–437 (2011).
4. Halvardson, J., Zaghlool, A. & Feuk, L. Exome RNA sequencing reveals rare and novel alternative transcripts. *Nucleic Acids Res.* **41,** e6–e6 (2013).
5. Clark, M. B. *et al.* The Reality of Pervasive Transcription. *PLoS Biol* **9,** e1000625 (2011).
6. Solomon, K. V., Haitjema, C. H., Thompson, D. A. & O'Malley, M. A. Extracting data from the muck: deriving biological insight from complex microbial communities and non-model organisms with next generation sequencing. *Current Opinion in Biotechnology* **28,** 103–110 (2014).
7. Wan, Y.-W., Mach, C. M., Allen, G. I., Anderson, M. L. & Liu, Z. On the Reproducibility of TCGA Ovarian Cancer MicroRNA Profiles. *PLoS ONE* **9,** e87782 (2014).
8. Fu, G. K. *et al.* Molecular indexing enables quantitative targeted RNA sequencing and reveals poor efficiencies in standard library preparations. *Proc. Natl. Acad. Sci. U.S.A.* **111,** 1891–1896 (2014).
9. Tan, W., Wang, K. & Drake, T. J. Molecular beacons. *Current Opinion in Chemical Biology* **8,** 547–553 (2004).
10. Geiss, G. K. *et al.* Direct multiplexed measurement of gene expression with color-coded probe pairs. *Nat Biotech* **26,** 317–325 (2008).
11. Sui, B., Li, L., Li, L. & Jin, W. An ultra-sensitive DNA assay based on single-molecule detection coupled with hybridization accumulation and its application. *The Analyst* **136,** 3950 (2011).
12. Østergaard, M. E. & Hrdlicka, P. J. Pyrene-functionalized oligonucleotides and locked nucleic acids (LNAs): Tools for fundamental research, diagnostics, and nanotechnology. *Chem. Soc. Rev.* **40,** 5771–5788 (2011).
13. Trcek, T. *et al.* Single-mRNA counting using fluorescent in situ hybridization in budding yeast. *Nat. Protocols* **7,** 408–419 (2012).

14. Zhang, D. Y., Chen, S. X. & Yin, P. Optimizing the specificity of nucleic acid hybridization. *Nat Chem* **4,** 208–214 (2012).

15. Gunnarsson, A., Jonsson, P., Marie, R., Tegenfeldt, J. O. & Hook, F. Single-Molecule Detection and Mismatch Discrimination of Unlabeled DNA Targets. *Nano Lett.* **8,** 183–188 (2008).

16. Ho, S.-L., Chan, H.-M., Ha, A. W.-Y., Wong, R. N.-S. & Li, H.-W. Direct Quantification of Circulating miRNAs in Different Stages of Nasopharyngeal Cancerous Serum Samples in Single Molecule Level with Total Internal Reflection Fluorescence Microscopy. *Anal. Chem.* **86,** 9880–9886 (2014).

17. Tan, G. C. *et al.* 5′ isomiR variation is of functional and evolutionary importance. *Nucl. Acids Res.* **42,** 9424–9435 (2014).

18. Ozsolak, F. *et al.* Amplification-free digital gene expression profiling from minute cell quantities. *Nat Meth* **7,** 619–621 (2010).

19. Kapranov, P. *et al.* New class of gene-termini-associated human RNAs suggests a novel RNA copying mechanism. *Nature* **466,** 642–646 (2010).

20. Jungmann, R. *et al.* Multiplexed 3D cellular super-resolution imaging with DNA-PAINT and Exchange-PAINT. *Nat Meth* **11,** 313–318 (2014).

21. Levene, M. J. *et al.* Zero-Mode Waveguides for Single-Molecule Analysis at High Concentrations. *Science* **299,** 682–686 (2003).

22. Cisse, I. I., Kim, H. & Ha, T. A rule of seven in Watson-Crick base-pairing of mismatched sequences. *Nat Struct Mol Biol* **19,** 623–627 (2012).

23. Dupuis, N. F., Holmstrom, E. D. & Nesbitt, D. J. Single-Molecule Kinetics Reveal Cation-Promoted DNA Duplex Formation Through Ordering of Single-Stranded Helices. *Biophysical Journal* **105,** 756–766 (2013).

24. Michelotti, N., de Silva, C., Johnson-Buck, A. E., Manzo, A. J. & Walter, N. G. A Bird's Eye View: Tracking Slow Nanometer-Scale Movements of Single Molecular Nano-Assemblies. *Methods Enzymol.* **475,** 121–148 (2010).